Physics and Imaging in Radiation Oncology 7 (2018) 51–57

Contents lists available at ScienceDirect

Physics and Imaging in Radiation Oncology

journal homepage: www.elsevier.com/locate/phro

Original Research Article

Comparison of time curves from dynamic ^{18}F-fluciclovine positron emission tomography and dynamic contrast-enhanced magnetic resonance imaging for primary prostate carcinomas

Andreas Julius Tulipan[a,b], Ljiljana Vlatkovic[c], Eirik Malinen[d,e], Bjørn Brennhovd[f], Knut Håkon Hole[a], Agnes Kathrine Lie[g], Harald Bull Ragnum[h,i], Mona-Elisabeth Revheim[a], Therese Seierstad[j,*]

[a] Department for Nuclear Medicine, Oslo University Hospital, Oslo, Norway
[b] Faculty of Clinical Medicine, University of Oslo, Oslo, Norway
[c] Department of Pathology, Oslo University Hospital, Oslo, Norway
[d] Department of Physics, University of Oslo, Oslo, Norway
[e] Department of Medical Physics, Oslo University Hospital, Oslo, Norway
[f] Department of Urology, Oslo University Hospital, Oslo, Norway
[g] Department of Pathology, Kalnes Hospital, Grålum, Norway
[h] Department of Radiation Biology, Oslo University Hospital, Oslo, Norway
[i] Clinic for Internal Medicine, Telemark Hospital Trust, Skien, Norway
[j] Department for Research and Development, Division for Radiology and Nuclear Medicine, Oslo University Hospital, Oslo, Norway

ARTICLE INFO

Keywords:
Prostate carcinoma
Fluciclovine
FACBC
MRI
Uptake characteristics

ABSTRACT

Background and purpose: Multimodal imaging is increasingly included in the assessment of prostate cancer patients, and there is a need to study whether different techniques provide similar or complementary information. In the initial perfusion phase contrast agents and radioactive labelled tracers act as blood-pool agents and may show similar characteristics. The purpose of the current work was to compare time-activity- and time-concentration-curves (TCs) of dynamic ^{18}F-fluciclovine (^{18}F-anti-1-amino-2-[F]-fluorocyclobutane-1-carboxylic acid, FACBC) positron emission tomography (PET) and dynamic contrast-enhanced magnetic resonance imaging (DCE MRI).

Materials and methods: Dynamic FACBC PET and DCE MRI were performed on 22 patients with intermediate or high-risk prostate cancer within 23 days prior to robot-assisted laparoscopic prostatectomy. Index tumour was delineated in the images using whole mount tissue sections as reference standard. Tumour TCs from PET and MRI were compared visually and quantitatively by calculating correlation coefficients between the curves at different time points after injection.

Results: For the first minute post injection, the mean correlation coefficient between the TCs from PET and MRI was 0.92 (range; 0.75–0.99). After the first minute, MRI showed washout while PET showed plateau kinetics.

Conclusion: Dynamic FACBC and DCE MRI showed similar wash-in time curve characteristics. At later time points, FACBC plateaued whereas MR contrast medium washed out. In DCE MRI, the usefulness of wash-in information is well documented. Whether wash-in information from dynamic FACBC can provide added value remains to be documented.

1. Introduction

Prostate carcinoma is the most common type of cancer in men and the second leading cause of cancer death in the Western world [1]. Prostate carcinomas are characterized by biological heterogeneous behaviour. While some tumours remain indolent for many years, others progress rapidly to a life-threatening disease. Due to this heterogeneity, an increasing number of imaging modalities are included in the diagnostic work-up of these patients. There is a need to establish to what extent different imaging modalities provide similar or complementary information.

The discovery of angiogenesis as an essential step for tumour growth has led to increasing interest in non-invasive assessment of tumour vasculature. Blood perfusion, blood volume, and vascular

* Corresponding author.

https://doi.org/10.1016/j.phro.2018.09.003
Received 9 May 2018; Received in revised form 20 September 2018; Accepted 20 September 2018

permeability can be visualized through analyses of time-activity- and time-concentration-curves (TCs) obtained by continuous acquisition of 2D or 3D image series during the uptake and clearance of a tracer or a contrast agent. Dynamic contrast-enhanced magnetic resonance imaging (DCE MRI) may be applied for prostate imaging as part of multiparametric MRI (mpMRI) for detection and characterization of tumour foci [2–5]. The TC on DCE MRI after administration of a Gadolinium-chelated contrast agent reflects the underlying tumour vasculature. The three main characteristic TCs are persistently enhancing (type I curve), plateau (type II curve) or washout (type III), with type III being most suggestive of malignancy [4]. It has been reported that rate of uptake obtained from the initial phase of DCE MRI may improve tumour detection and differentiate low-grade from high-grade tumours [5,6].

^{18}F-labeled fluciclovine (also known as anti-1-amino-2-[F]-fluorocyclobutane-1-carboxylic acid (FACBC), brand name; Axumin) is a new PET tracer that was recently approved by The Food and Drug Administration (FDA) and The European Medicines Agency (EMA) for use in patients with suspected prostate cancer recurrence. The uptake mechanism of FACBC into cells is not fully understood, but it has been reported to primarily be mediated by the two amino acid transporter proteins ASCT2 and LAT1 [7,8]. The expression of ASCT2 and LAT1 is linked to prostate cancer aggressiveness [9], and FACBC PET could thus improve treatment stratification. Monitoring delivery and retention of FACBC from the time of injection provide dynamic image series that enable separation of perfusion [10,11] from more specific tracer distribution characteristics such as tracer-transport, binding and metabolism.

In the initial perfusion phase contrast agents and radioactive labelled tracers act as blood-pool agents, whereas tissue distribution and uptake depend on the chemical and biological properties of these agents. A prostate cancer study with dynamic ^{18}F-fluorodeoxyglucose (FDG) PET/MR revealed a possible additional value of dynamic PET [12]. There are some studies with dynamic FACBC PET/CT [13–18], but only two have explored the early dynamic phase [16,17]. None of these studies assessed if the dynamic information was similar to DCE MRI. One dynamic PET/MR study with ^{18}F-fluciclovine focused at finding the optimal time point to detect prostate cancer, but did not evaluate initial PET perfusion in detail and did not include DCE MRI [19]. Comparison of perfusion characteristics from DCE MRI and dynamic FACBC PET is lacking.

Hypoxia is associated with treatment resistance to radiotherapy. Accordingly, it could be beneficial to include perfusion information from PET in dose painting. MpMRI including DCE is currently used in clinical radiotherapy trials to guide focal boosting of prostate cancer [20,21]. Reliable mapping and characterization of the resistant lesion (s) within the prostate gland is a prerequisite for these strategies, and perfusion information may complement the metabolic information from PET.

The aim of the present study was to compare the TCs from DCE MRI and dynamic ^{18}F-FACBC PET for primary localized prostate carcinomas.

2. Material and methods

2.1. Study cohort

A total of 22 patients with intermediate or high-risk prostate carcinoma according to ÓAmico risk classification [22] referred to our institution for robot-assisted laparoscopic prostatectomy (RALP) between February 2013 and May 2016 were included in this prospective study. Patient and tumour characteristics are shown in Supplementary Table 1. The median age of the study cohort was 67 years (range; 46–74). Prostate specific antigen (PSA) ranged from 4.6 to 37 ng/mL (median; 8.9). Of the 22 patients, eight had Gleason score < 7b and 15 had tumour growth beyond the confines of the prostate (extracapsular extension). Both MRI and PET were performed less than 23 days prior to RALP. The mean time between MRI and PET was 5.4 days (range: 1–14 days). The Regional Committees for Medical and Health Research Ethics South East approved the study (REC 2010/1656). The study was carried out in accordance with the Helsinki Declaration and all patients provided written informed consent before study inclusion.

2.2. MRI

The MRI examinations were performed with a 1.5T MR scanner (GE Horizon, GE Healthcare, Waukesha, Wisconsin) and a phased array cardiac coil centred over the pelvis. The mpMRI examinations included morphological and functional sequences according to international recommendations [2] (Supplementary Table 2). The transversal DCE MR images were acquired with a 3D spoiled GE-Dixon sequence (Time to echo (TE) = 3.1 ms, time to repetition (TR) = 5.8 ms, field of view (FOV) = 240 × 240 mm^2, acquisition/reconstruction matrix = 160 × 160/256 × 256, number of slices = 10, voxel size = 1.5 × 1.5 × 2.6 mm^3, parallel imaging factor = 2). A total of 30 T1-weighted acquisitions were sequentially obtained with 11.4 s temporal resolution. Gadolinium contrast medium (gadoterate meglumine) was injected as an intravenous bolus at the start of the fourth dynamic scan through a peripherally placed cannula using an automatic injector (0.2 ml/kg body mass, 3 ml/s flow rate, Dotarem® (279.3 mg/ml, Guerbet, France)) and followed by 30 ml saline flush.

2.3. Dynamic ^{18}F-fluciclovine PET

FACBC PET and computed tomography (CT) images were acquired with a Biograph40 mCT (Siemens, Erlangen, Germany). The patients fasted for at least four hours and voided the bladder before the examination. A helical CT scan (CareDose 4D eff. 82 mAs, tube voltage = 120 kV, FOV = 78 cm, matrix size = 512 × 512, slice thickness = 1.5 mm) of the pelvis for attenuation correction was followed by intravenous bolus administration of 281–301 MBq FACBC and saline flush of 10–20 ml. A 15 min list-mode PET acquisition of one bed position (axial FOV of 21.6 cm centred above the symphysis, PET ring diameter FOV = 70 cm) was started before administration of FACBC. The list-mode data was rebinned into image time frames of 15 s for the first three minutes, 30 s for the next 1.5 min, 2 min for the next, and then 4 min for the remaining time. The images were reconstructed using 3D iterative ordered-subset expectation maximization (OSEM) with 2 iterations and 21 subsets, time of flight (TOF), point-spread function (PSF)-correction, slice thickness 1.5 mm, matrix size 128 × 128, in-plane reconstruction pixels size 5.5 mm × 5.5 mm, and a Gaussian post-reconstruction convolution kernel with full width at half maximum (FWHM) of 3 mm. All studies were transferred to a remote PC for further analyses.

2.4. Robot-assisted laparoscopic prostatectomy

All patients underwent RALP with a three-armed robotic DaVinci® system (Intuitive Surgical, Sunnyvale, CA, USA) with the surgical approach mainly based on the Vattikutti Institute technique [23]. The median number of days between MRI and RALP was 4.4 days (range 0–23) and between PET and RALP 9.8 days (range 1–18).

2.5. Histopathological assessment of tissue sections from resected prostate glands

The resected prostate was inked with three colours to identify left, right, and posterior aspects and fixed in 10% buffered formaldehyde for at least two days. Grossing was performed according to a standardized protocol where total prostate with seminal vesicles was embedded [24]. The apex and the base of the prostate were cut as sagittal sections using the cone method. The remaining body was cut into three to four mm transverse slices and prepared as whole-mount sections. The sections were stained with hematoxylin and eosin (HE) and examined by light

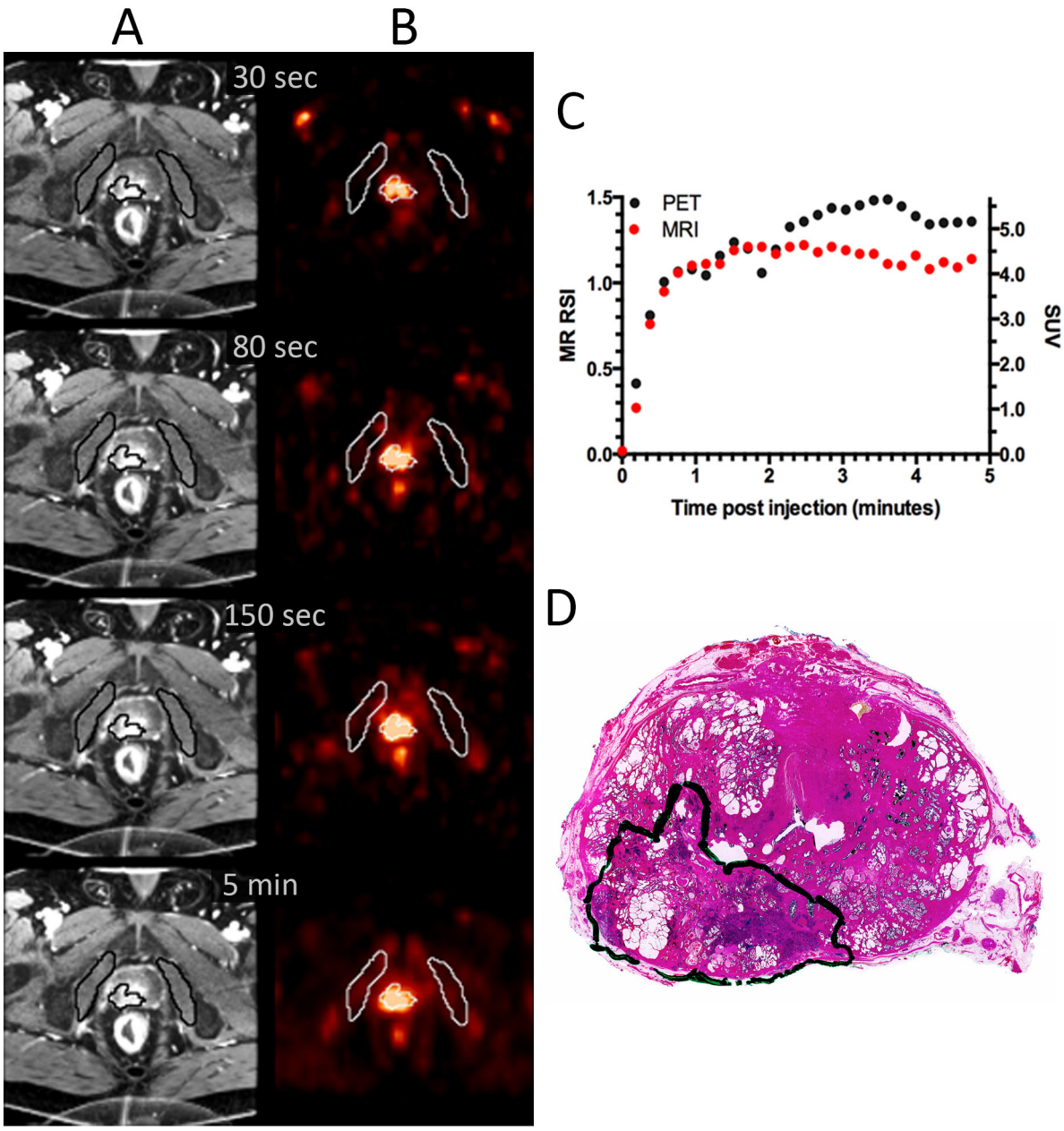

Fig. 1. Dynamic MRI (A), dynamic FACBC PET (B), uptake curves from MRI and PET (C) from the tumour outlined in the corresponding HE stain of the prostate gland (D) for a patient with T3a, Gleason score 7b tumour.

microscopy by two experienced uropathologists (LV and AKL), blinded to the imaging results. Histopathological assessment included staging according to the 7th edition TNM classification [25] and determination of Gleason score [26]. The index tumour was defined in descending order as: tumour with extracapsular extension, the highest Gleason score or largest extent. The index tumour was delineated by the pathologist (Fig. 1D and Supplementary Fig. 1D).

2.6. Data analyses

An experienced MR prostate radiologist (KHH) [27,28] contoured the index lesion in the MR images based on the pathologists' delineations in the corresponding whole-mount HE-sections. The delineation was guided by internal landmarks such as the urethra and ejaculatory ducts and relative distances from the midline, surgical capsule, and outer prostatic margin [29]. Because the HE sections and the MR slices never are identical the delineated ROI was defined as the union of the tumour extent at histopathology and MRI. The internal obturator muscles next to the prostate gland were also delineated to aid in the co-registration of the images. All ROI files were saved for further processing as described below.

All image analyses were performed with in-house developed software written in Interactive Data Language (IDL 8.4, Harris Geospatial Solutions, Broomfield, USA) codes. MR, PET and CT images were imported into IDL and all images were rebinned to a common isotropic voxel size of 3 mm × 3 mm × 3 mm. For the PET images, SUV was calculated for each voxel by dividing the voxel concentration by the injected activity per body weight. For the MR time series, relative signal

intensity (RSI) images were constructed by taking the signal intensity difference between time point *i* and the mean of the pre-contrast images divided by the mean pre-contrast signal intensity. Here, it is assumed that RSI is approximately proportional to the tissue concentration of gadoterate meglumine [30,31]. Then, the PET images were linearly interpolated to yield the same temporal resolution as the MR series. The entire prostate gland was delineated in the MR images and this 3D volume of interest (VOI) was transferred to the CT images. The VOI from MR was manually shifted to match the prostate gland in the CT images. The shift coordinates obtained from this matching was used to bring the MR and the PET images into the same spatial coordinate frame. In cases of misalignment of the prostate arising from patient or bowel movement in the resulting PET/MR images, the PET space was manually adjusted in 3D before further processing. With the image series co-registered, the mean signal in the tumour ROI at MRI and PET was extracted for each time point. The TCs were shifted so that the 0th time point was the latest time point where no tracer was seen in the tissue. The Pearson correlation coefficient was used to compare the TCs from PET and MRI for individual patients.

Associations between FACBC uptake in the tumour in the initial perfusion phase (45 s post injection) and in the metabolic phase (4–6 min post injection) were compared to PSA, pathological tumour stage and Gleason score using correlation analyses. The significance level was set to 5%.

3. Results

Fig. 1 and Supplementary Fig. 1 show axial images from dynamic MRI and PET, the tumour TCs and the corresponding histological tissue sections for two of the patients. In Fig. 1, the tumour was clearly distinguishable from the surrounding benign tissue at all time points for MRI and PET. The TCs for both modalities showed an initial rapid wash-in and a plateau curve (type II). The correlation coefficient between the TCs for the two modalities was 0.92 for the initial five minutes post injection (Fig. 1).

In the initial phase, the cohort-based mean TCs from DCE MRI and FACBC PET both showed rapid wash-in (Fig. 2). After initial wash-in, the MR contrast media was cleared from the tumour tissue whereas FACBC was retained in the tumour.

In the early perfusion phase there was a strong and significant correlation between FACBC uptake and MR contract agent uptake for individual patients (mean; 0.92, range; 0.75–0.99, Fig. 3). At later time points the correlations decreased and in the time interval from 1.5 to 5 min post injection the mean correlation coefficient was 0.33 (range; 0.02–0.84) with the correlation being significant for only seven of the 22 patients. The mean correlation coefficient for these seven patients was 0.60. There were no significant correlations between FACBC uptake and PSA, pathological tumour stage and Gleason score (Fig. 4).

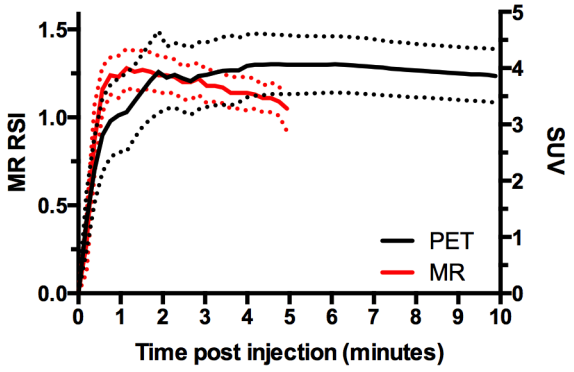

Fig. 2. Population-based TCs from DCE MRI and ^{18}F-FACBC PET SUV. The cohort included 22 primary prostate tumours. Data are given as mean and standard deviation.

4. Discussion

In the present study we compared the TCs from dynamic FACBC PET and DCE MRI for 22 primary prostate carcinomas. Both imaging modalities showed highly similar initial wash-in. At later time-points, MR contrast agent washed out, whereas FACBC was retained in the extravascular compartment(s).

Due to physiological differences in the uptake of FACBC and MR contrast agents, differences in kinetic characteristics were anticipated. For blood pool agents without exchange between the vascular and the extravascular space the TCs would resemble an arterial input function with a rapid wash-in followed by a bi-exponential rapidly decaying curve [32]. In the initial phase, both FACBC and gadoterate meglumine act as blood pool agents confined within the vasculature, giving rise to an initial rapid signal increase in the images. When the bolus reaches the tissue, the tracer enters the extravascular extracellular space through passive diffusion. For FACBC there may also be a component of active transport across the endothelial lining of the vascular membrane [33]. Following renal clearance, the diffusion of Gadolinium-contrast was reversed and TC type II or III was observed for all except one tumour. The build-up phase of FACBC starts at the same time as the peak from the initial bolus infusion appears. FACBC is transported across the endothelium and tissue cell membranes by passive diffusion and mediated by the amino acid transporters ASCT2 and LAT1 [7,8]. FACBC is not incorporated into proteins and is not metabolized significantly [8]. The amino acid transport via LAT1 is expected to be a 1:1 exchange [34], and thus the FACBC uptake in tumour tissue should decline with time. However, the expected decrease in uptake was observed only in a few of the patients. It has been reported that equilibrium occurs around 30 min after injection, and thus, our limited PET acquisition time could explain why decrease was not seen in more patients [14,19]. Principally, the accumulation of a PET tracer can be seen as a sum of three components: (1) A vascular component with TC characteristics similar to what is seen in an artery, (2) an extravascular-extracellular component and (3) an intracellular component. Accumulation in the intracellular compartment may occur even if the intravascular and the extravascular-extracellular components are diminishing. The observed plateau curve indicates that FACBC accumulates and that there is not a 1:1 exchange with the extravascular-extracellular space.

In the initial perfusion phase, there was a strong correlation between the TCs from DCE MRI and the TCs from dynamic FACBC PET. One may speculate if the perfusion information can improve the performance of FACBC PET. Dynamic FACBC PET would probably not improve the detection of primary prostate cancer because DCE MRI (mainly reflecting perfusion) has a minor role in this setting [3]. Also, the metabolic phase of FACBC PET has shown limited accuracy [14,16]. In contrast, the initial phase of dynamic FACBC PET might improve the detection of local recurrences because DCE MRI has an essential role in this setting [35,36]. Moreover, static FACBC PET has shown promising results [37] and is already approved by FDA and EAM for this indication.

The strengths of our study include short time between MRI, PET and surgery, and the whole-mount tissue sections from radical prostatectomy specimens as reference standard. Our study has several limitations: The relatively small patient cohort limits the generalizability of the study results. The MR and the PET images had different voxel sizes and extensive downsampling and interpolation of the MR images were performed to match the spatial resolution of the PET images. PET images with smaller voxels were explored, but rejected due to low number of counts in the different time frames. Large difference in

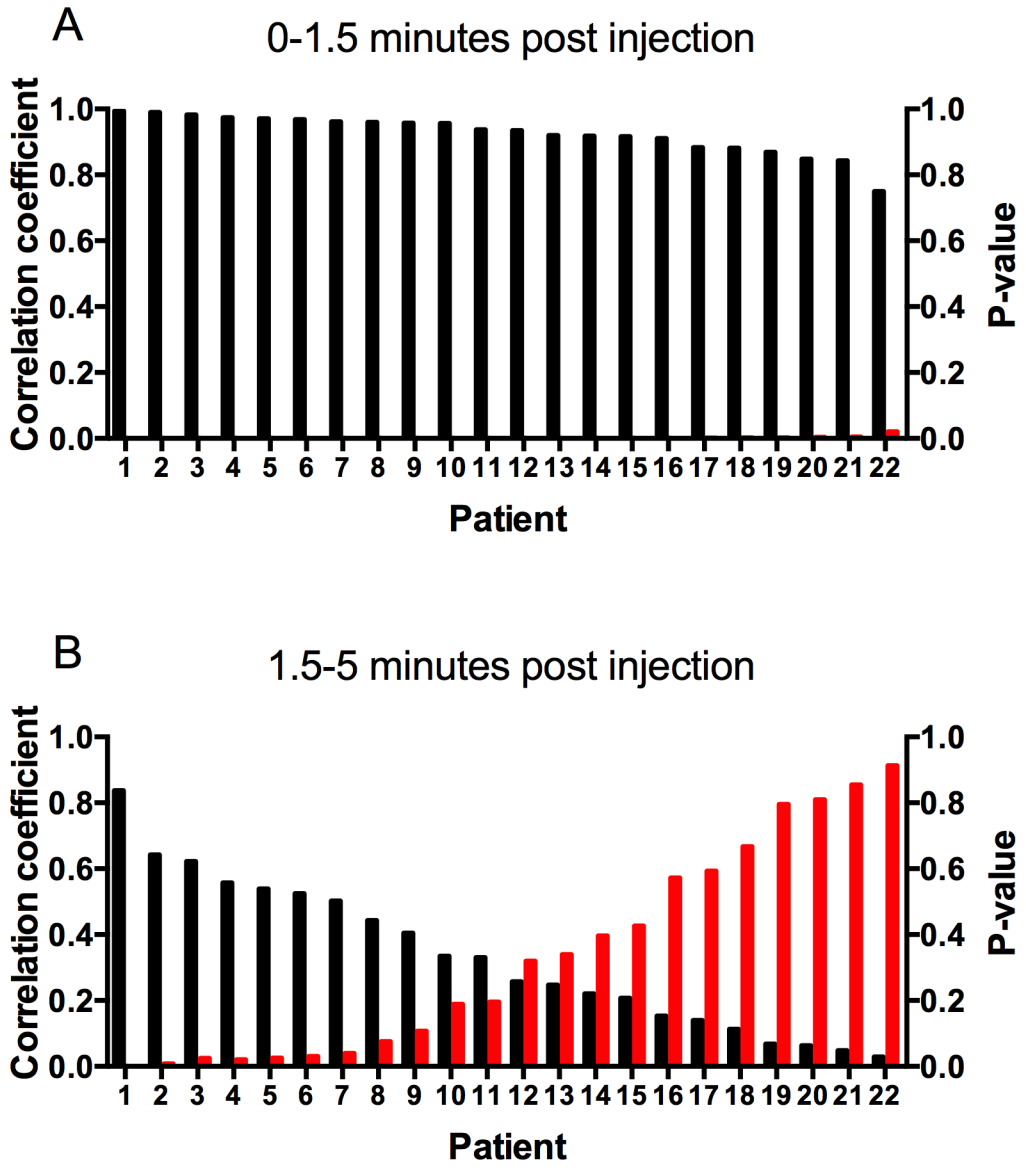

Fig. 3. Pearson correlation coefficient (black bars) between tumour TCs from DCE MRI and dynamic FACBC PET for individual patients for 0–1.5 (A) and 1.5–5 min post injection (B). Red bars represent the p-values. (For interpretation of the references to colour in this figure legend, the reader is referred to the web version of this article.)

spatial resolution between the modalities and low signal-to-noise ratio of the PET images hampered comparison of spatial uptake heterogeneity. We therefore chose to compare the mean tumour TCs to minimize the influence of measurement uncertainty. We manually transferred the histopathologically defined tumour ROI to the MR images, which introduce concerns. The HE-sections and the MR slices are never identical. Our approach ensured that the ROI in the MR images only comprised tumour, but the entire tumour was not necessarily included. For the comparison of the TCs, exact co-registration of MRI and PET is probably more critical than matching of histopathology and MRI.

In conclusion, in the initial phase after intravenous administration the TCs from FACBC PET and DCE MRI both showed rapid wash-in. At later time points, FACBC accumulated in the extravascular compartment(s), while the MR contrast medium washed out.

5. Contribution

Conception and design of the study (AJT, LV, EM, BB, KHH, AKL, HBR, MER, TS), acquisition of data (AJT, LV, EM, BB, KHH, AKL, HBR, TS), analysis and interpretation of the data (AJT, EM, MER, TS), drafting the article (AJT, EM, TS), revising the article critically for intellectual content (LV, BB, KHH, HBR, AKL, MER), final approval of the submitted version (AJT, LV, AKL, BB, KHH, HBR, EM, MER, TS).

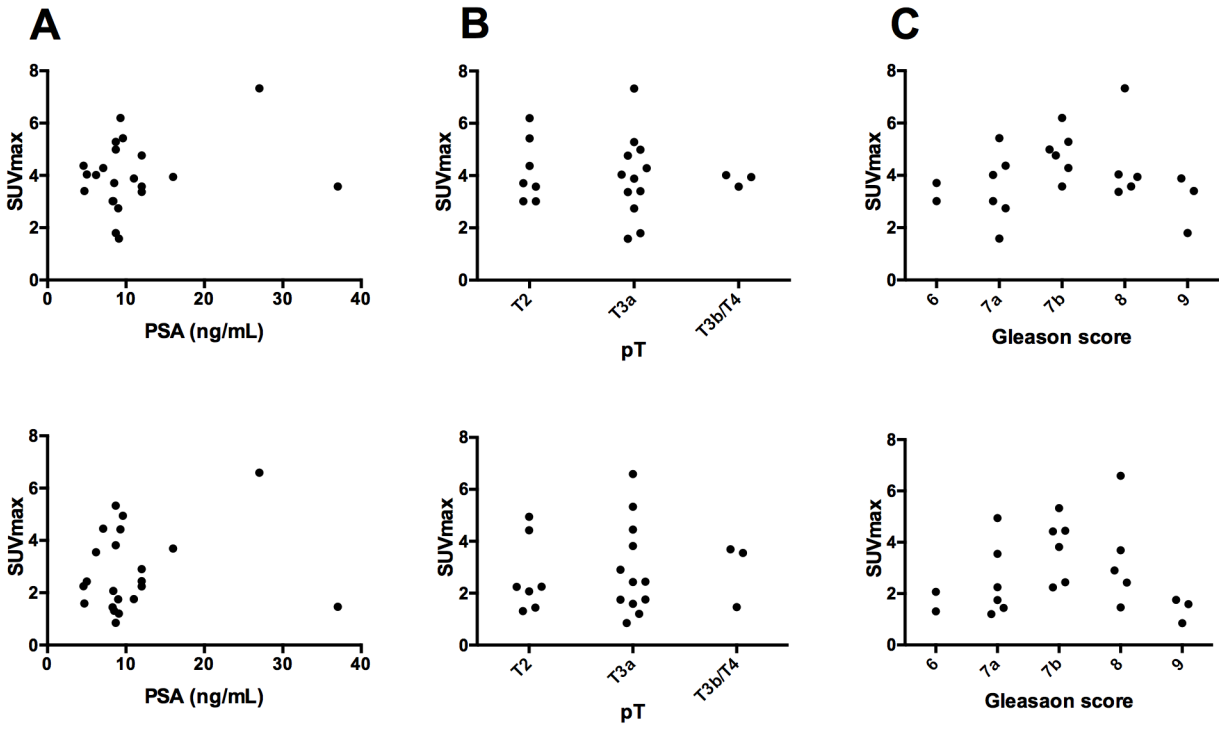

Fig. 4. FACBC uptake against prostate specific antigen (PSA) (A), pathological tumour stage (pT) (B) and Gleason score (C). The metabolic phase (upper panel) and the initial perfusion phase (bottom panel) of dynamic FACBC PET.

Disclosure of potential conflicts of interest

All authors declare no conflict of interest.

Acknowledgement

H.B. Ragnum was supported by the European Union 7th Framework program (grant no. 222741-METOXIA). T. Seierstad was supported by the Norwegian Cancer Society (grant no. 419340) and the Comprehensive Cancer Center at the Radium Hospital.

Appendix A. Supplementary data

Supplementary data to this article can be found online at https://doi.org/10.1016/j.phro.2018.09.003.

References

[1] Siegel RL, Miller KD, Jemal A. Cancer statistics, 2016. CA Cancer J Clin 2016;66:7–30.
[2] Barentsz JO, Richenberg J, Clements R, Choyke P, Verma S, Villeirs G, et al. ESUR prostate MR guidelines 2012. Eur Radiol 2012;22:746–57.
[3] Barentsz JO, Weinreb JC, Verma S, Thoeny HC, Tempany CM, Shtern F, et al. Synopsis of the PI-RADS v2 guidelines for multiparametric prostate magnetic resonance imaging and recommendations for use. Eur Urol 2016;69:41–9.
[4] Bonekamp D, Macura KJ. Dynamic contrast-enhanced magnetic resonance imaging in the evaluation of the prostate. Top Magn Reson Imaging 2008;19:273–84.
[5] Hotker AM, Mazaheri Y, Aras O, Zheng J, Moskowitz CS, Gondo T, et al. Assessment of prostate cancer aggressiveness by use of the combination of quantitative DWI and dynamic contrast-enhanced MRI. AJR Am J Roentgenol 2016;206:756–63.
[6] Vos EK, Litjens GJ, Kobus T, Hambrock T, Hulsbergen-van de Kaa CA, Barentsz JO, et al. Assessment of prostate cancer aggressiveness using dynamic contrast-enhanced magnetic resonance imaging at 3 T. Eur Urol 2013;64:448–55.
[7] Oka S, Okudaira H, Yoshida Y, Schuster DM, Goodman MM, Shirakami Y. Transport mechanisms of trans-1-amino-3-fluoro[1-(14)C]cyclobutanecarboxylic acid in prostate cancer cells. Nucl Med Biol 2012;39:109–19.
[8] Okudaira H, Shikano N, Nishii R, Miyagi T, Yoshimoto M, Kobayashi M, et al. Putative transport mechanism and intracellular fate of trans-1-amino-3-18F-fluorocyclobutanecarboxylic acid in human prostate cancer. J Nucl Med 2011;52:822–9.
[9] Segawa A, Nagamori S, Kanai Y, Masawa N, Oyama T. L-type amino acid transporter 1 expression is highly correlated with Gleason score in prostate cancer. Mol Clin Oncol 2013;1:274–80.
[10] Mullani NA, Herbst RS, O'Neil RG, Gould KL, Barron BJ, Abbruzzese JL. Tumor blood flow measured by PET dynamic imaging of first-pass 18F-FDG uptake: a comparison with 15O-labeled water-measured blood flow. J Nucl Med 2008;49:517–23.
[11] Cochet A, Pigeonnat S, Khoury B, Vrigneaud JM, Touzery C, Berriolo-Riedinger A, et al. Evaluation of breast tumor blood flow with dynamic first-pass 18F-FDG PET/CT: comparison with angiogenesis markers and prognostic factors. J Nucl Med 2012;53:512–20.
[12] Rosenkrantz AB, Koesters T, Vahle AK, Friedman K, Bartlett RM, Taneja SS, et al. Quantitative graphical analysis of simultaneous dynamic PET/MRI for assessment of prostate cancer. Clin Nucl Med 2015;40:e236–40.
[13] Schuster DM, Votaw JR, Nieh PT, Yu W, Nye JA, Master V, et al. Initial experience with the radiotracer anti-1-amino-3-18F-fluorocyclobutane-1-carboxylic acid with PET/CT in prostate carcinoma. J Nucl Med 2007;48:56–63.
[14] Schuster DM, Taleghani PA, Nieh PT, Master VA, Amzat R, Savir-Baruch B, et al. Characterization of primary prostate carcinoma by anti-1-amino-2-[(18)F]-fluorocyclobutane-1-carboxylic acid (anti-3-[(18)F] FACBC) uptake. Am J Nucl Med Mol Imaging 2013;3:85–96.
[15] Schuster DM, Nieh PT, Jani AB, Amzat R, Bowman FD, Halkar RK, et al. Anti-3-[(18)F]FACBC positron emission tomography-computerized tomography and (111) In-capromab pendetide single photon emission computerized tomography-computerized tomography for recurrent prostate carcinoma: results of a prospective clinical trial. J Urol 2014;191:1446–53.
[16] Turkbey B, Mena E, Shih J, Pinto PA, Merino MJ, Lindenberg ML, et al. Localized prostate cancer detection with 18F FACBC PET/CT: comparison with MR imaging and histopathologic analysis. Radiology 2014;270:849–56.
[17] Sorensen J, Owenius R, Lax M, Johansson S. Regional distribution and kinetics of [18F]fluciclovine (anti-[18F]FACBC), a tracer of amino acid transport, in subjects with primary prostate cancer. Eur J Nucl Med Mol Imaging 2013;40:394–402.
[18] Nye JA, Schuster DM, Yu W, Camp VM, Goodman MM, Votaw JR. Biodistribution and radiation dosimetry of the synthetic nonmetabolized amino acid analogue anti-18F-FACBC in humans. J Nucl Med 2007;48:1017–20.
[19] Elschot M, Selnaes KM, Sandsmark E, Kruger-Stokke B, Storkersen O, Tessem MB, et al. A PET/MRI study towards finding the optimal [(18)F]Fluciclovine PET protocol for detection and characterisation of primary prostate cancer. Eur J Nucl Med Mol Imaging 2017;44:695–703.
[20] Monninkhof EM, van Loon JWL, van Vulpen M, Kerkmeijer LGW, Pos FJ, Haustermans K, et al. Standard whole prostate gland radiotherapy with and without lesion boost in prostate cancer: Toxicity in the FLAME randomized controlled trial. Radiother Oncol 2018;127:74–80.
[21] Haworth A, Williams S. Focal therapy for prostate cancer: the technical challenges. J Contemp Brachytherapy 2017;9:383–9.
[22] D'Amico AV, Whittington R, Malkowicz SB, Schultz D, Blank K, Broderick GA, et al.

Biochemical outcome after radical prostatectomy, external beam radiation therapy, or interstitial radiation therapy for clinically localized prostate cancer. JAMA 1998;280:969–74.
[23] Tewari A, Peabody J, Sarle R, Balakrishnan G, Hemal A, Shrivastava A, et al. Technique of da Vinci robot-assisted anatomic radical prostatectomy. Urology 2002;60:569–72.
[24] Srigley JR. Key issues in handling and reporting radical prostatectomy specimens. Arch Pathol Lab Med 2006;130:303–17.
[25] Sobin LHG, Gospodarowicz MK, Wittekind CTNM. Classification of malignant tumours. 7th ed. Chichester: Wiley-Blackwell; 2011.
[26] Epstein JI. An update of the Gleason grading system. J Urol 2010;183:433–40.
[27] Hole KH, Axcrona K, Lie AK, Vlatkovic L, Geier OM, Brennhovd B, et al. Routine pelvic MRI using phased-array coil for detection of extraprostatic tumour extension: accuracy and clinical significance. Eur Radiol 2013;23:1158–66.
[28] Hole KH, Larsen SG, Groholt KK, Giercksky KE, Ree AH. Magnetic resonance-guided histopathology for improved accuracy of tumor response evaluation of neoadjuvant treatment in organ-infiltrating rectal cancer. Radiother Oncol 2013;107:178–83.
[29] Groenendaal G, Moman MR, Korporaal JG, van Diest PJ, van Vulpen M, Philippens ME, et al. Validation of functional imaging with pathology for tumor delineation in the prostate. Radiother Oncol 2010;94:145–50.
[30] Evelhoch JL. Key factors in the acquisition of contrast kinetic data for oncology. J Magn Reson Imaging 1999;10:254–9.
[31] Tofts PS. Modeling tracer kinetics in dynamic Gd-DTPA MR imaging. J Magn Reson Imaging 1997;7:91–101.
[32] Canet EP, Casali C, Desenfant A, An MY, Corot C, Obadia JF, et al. Kinetic characterization of CMD-A2-Gd-DOTA as an intravascular contrast agent for myocardial perfusion measurement with MRI. Magn Reson Med 2000;43:403–9.
[33] Mann GE, Yudilevich DL, Sobrevia L. Regulation of amino acid and glucose transporters in endothelial and smooth muscle cells. Physiol Rev 2003;83:183–252.
[34] Meier C, Ristic Z, Klauser S, Verrey F. Activation of system L heterodimeric amino acid exchangers by intracellular substrates. EMBO J 2002;21:580–9.
[35] Panebianco V, Barchetti F, Barentsz J, Ciardi A, Cornud F, Futterer J, et al. Pitfalls in interpreting mp-MRI of the prostate: a pictorial review with pathologic correlation. Insights Imaging 2015;6:611–30.
[36] Barchetti F, Panebianco V. Multiparametric MRI for recurrent prostate cancer post radical prostatectomy and postradiation therapy. Biomed Res Int 2014;2014:316272.
[37] Schuster DM, Savir-Baruch B, Nieh PT, Master VA, Halkar RK, Rossi PJ, et al. Detection of recurrent prostate carcinoma with anti-1-amino-3-18F-fluorocyclobutane-1-carboxylic acid PET/CT and 111In-capromab pendetide SPECT/CT. Radiology 2011;259:852–61.